PAPER

Check for updates

Tetraarylethene fluorescent dyes with aggregation-induced emission for LED-driven photocuring and 3D printing†

Dongxiao Li,‡ Yimei Liu,‡ Binghui Bao, Yao Du, Jian You, Luhang Zhang, Haitao Zhan, Mingyang Li and Tao Wang ⓘ *

Four tetraarylethene-based fluorescent dyes (*i.e.*, Cz-bi-Ph, Cz-hex-Ph, DHBF-Ph, and BP-Ph) with aggregation-induced emission (AIE) properties were synthesized. The fluorescence properties of the dyes in the liquid (solution) and solid states during the photocuring process were characterized. Their sensitizing activity to the photoinitiator in the LED-driven photocuring of acrylic monomer and epoxy resin was investigated. In the photocuring system initiated by photoinitiator diphenyl(2,4,6-trimethylbenzoyl)-phosphine oxide (TPO), all the dyes showed good photostability and fluorescence enhancement within the irradiation period. Dyes can be used to successfully obtain solid-state fluorescent samples from digital light processing 3D printing that can be used as the fluorescent probe to monitor the photocuring process. The obtained tetraarylethene-based fluorescent dyes were found to have photosensitization properties for photoinitiator diaryliodonium salt (ONI) under a 405 nm LED and can initiate the curing of acrylate monomer and epoxy oligomer. In the photocuring system initiated by dye-sensitized ONI, Cz-bi-Ph and Cz-hex-Ph showed a strong photosensitization activity. The sensitization activities of DHBF-Ph and BP-Ph were relatively weak. However, the fluorescence of the corresponding systems, which can be used as both fluorescent probes and sensitizers, changed significantly with the photocuring process, and their fluorescence tended to be stable when the photocuring was completed.

Introduction

Conferring new functionalities to polymeric materials using dyes is particularly advantageous because a small amount of dye could remarkably change the material's properties while retaining the mechanical features of the matrix.[1–4] In recent years, the capability of specific dyes to go beyond conventional use and confer functional properties to 3D printed objects has attracted research attention.[5–8] By modifying the elastic modulus under light irradiation, inducing optical and emission properties in the matrix, or providing temperature responsiveness which can amplify the molecular level and change the properties of materials,[9] functional 3D printing samples can be prepared by combining carefully designed dyes with an appropriate 3D printing matrix.[10–15]

For different 3D printing technologies, photocuring-based 3D printing techniques, mainly including digital light processing (DLP) and stereolithography (SLA) that use LEDs as light sources, have attracted widespread attention due to their green nature, which means the absence of organic solvents as volatile compounds (VOCs) and low energy consumption, high resolution, small size, and economic advantages.[16–19] SLA can print the required parts with a resolution as low as 10 μm. Compared to SLA, DLP has a faster printing speed but is limited by the resolution of the digital light mirror. Three-dimensional printable liquids in the DLP and SLA techniques have various components. Among them, dyes are usually underrated because they are introduced merely for aesthetical reasons, to enhance the objects' resolution, or as one of the components of the photoinitiator for sensitization and photoinitiation effects.[20–22] For example, Lalevée *et al.* prepared a 3D model by photocuring printing with a three-component photoinitiator (PIS) on the basis of dye/iodine/EDB.[23] Ortyl *et al.* reported the fluorescent solid obtained after a 3D printing experiment based on formulations with a fluorescent dye in the polymerization system.[24] He *et al.* prepared three luminescent resins and explored their resin composition and printing parameters through cured depth studies.[25]

Some traditional fluorescent dyes exhibit the aggregation-caused quenching (ACQ) phenomenon, such as rhodamine, coumarin, and pyrene, which exhibit noticeable fluorescence in the solution state but none in the solid state, significantly

Department of Organic Chemistry, College of Chemistry, Beijing University of Chemical Technology, Beijing, 100029, P. R. China.
E-mail: wangtwj2000@163.com; Tel: +86-010-64445350
† Electronic supplementary information (ESI) available. See DOI: **https://doi.org/10.1039/d2ma00280a**
‡ Dongxiao Li and Yimei Liu contributed equally to this manuscript.

limiting the application and development of solid luminescent materials.[26–30] The concept of aggregation-induced emission (AIE) first proposed by Tang *et al.* has attracted great attention.[31–34] In recent decades, the limitations of traditional CQ in applications have been overcome by the discovery of AIE molecules, which are used in fluorescent probes, 3D printing, biological imaging, sensing, and other fields.[35–38] The photocuring system doped with AIE fluorescent dyes can print solid materials with apparent fluorescence by 3D printing, allowing solid luminescent materials to be developed.[39,40] Our research group reported the use of anthracene-based dyes in iodonium salts to initiate free radical photocuring (FRP) and the use of the AIE properties of anthracene-based dyes to monitor the photocuring process.[41]

In the photocuring 3D printing, the aggregation of solid fluorescence quenching when printing fluorescent samples often occurs. The photocuring activity can be reduced due to the absorption of fluorescent dyes. To solve the above problems, we synthesized four AIE fluorescent dyes in this study, namely (*E*)-1,2-bis(9-ethyl-9*H*-carbazol-3-yl)-1,2-diphenylethene (Cz-bi-Ph), (*E*)-1,2-bis(9-ethyl-9*H*-carbazol-3-yl)-1,2-diphenylethene(Cz-bi-Ph), (*E*)-1,2-bis(2,3-dihydrobenzofuran-5-yl)-1,2-diphenyl- -ethene (DHBF-Ph), and (*E*)-1,2-di([1,1′-biphenyl]-4-yl)-1,2-diphenylethene (BP-Ph), by introducing aromatic amine groups and polycyclic aromatic hydrocarbons into the tetrastyrene scaffold. Their fluorescence properties and sensitizing activity in the photocuring of acrylic monomer and epoxy resin were investigated in the photocuring systems initiated by photoinitiator diphenyl(2,4,6-trimethylbenzoyl)-phosphine oxide (TPO) and dye-sensitized diaryliodonium salt (ONI), respectively. Solid state fluorescent samples were obtained and exhibited an appearance with high print fidelity through a DLP 3D printer.

Experimental part

Materials and characterization

The details of the materials are given in the ESI.† ^{1}H NMR (400 MHz) and ^{13}C NMR (101 MHz) spectra were recorded on a Bruker AV400 NMR spectrometer. IR spectra were recorded on a Nicolet 5700 instrument (Thermo Electron Corporation, Waltham, MA). The UV-vis spectra and steady-state photolysis experiments were recorded on a UV-5200 (UNICO) UV-vis spectrophotometer.

Cyclic voltammetric (CV) analysis was performed on a CHI660E electrochemical workstation. The cyclic voltammetry experiments were carried out in THF with 0.1 M n-Bu$_4$NPF$_6$ as the electrolyte, Ag/AgCl as the reference electrode, and ferrocene as the internal standard.

Photocuring system

In this work, Cz-bi-Ph, Cz-hex-Ph, DHBF-Ph, and BP-Ph were prepared as fluorescence dyes and added to the photocuring system for 3D printing fluorescence samples. Two kinds of photoinitiators were used. One photoinitiator in this study is TPO which can directly initiate the photocuring of acrylate monomers under a 405 nm LED. The other photoinitiator is ONI which needs dyes to photosensitize under a 405 nm LED. The incident light intensity at the sample surface was set at about 80 mW cm^{-2} for the 405 nm LED. Tripropylene glycol diacrylate (TPGDA), trimethylolpropane triacrylate (TMPTA), and polyethylene glycol diacrylate (PEGDA) were used as monomers for FRP, and diglycidyl ether of bisphenol A (E51) epoxy was used as a monomer for cationic photocuring (CP).

The double bond conversion rates and epoxy conversion rates in the photocuring system were recorded by a Nicolet 5700 instrument (Thermo Electron Corporation, Waltham, MA). The fluorescence change of the photocuring system was recorded by an F-4500 (Hitachi High-Technologies Corporation) fluorescence spectrophotometer. The details of photopolymerization are shown in the ESI.†

3D printing experiment

The 3D printing formula for obtaining solid luminescent materials is 0.5 wt% of dyes, 0.50 wt% of TPO, 1.0 wt% of NMP (*N*-methyl pyrrolidone, solvent for dissolving TPO and dyes), and 98.0 wt% of TPGDA. The solid luminescent materials were printed by a DLP 3D printer (Guang Lei Intelligent Manufacturing Co, Ltd, Foshan, PR China). The power of the 405 nm LED during the printing process is 4 mW cm^{-2}. We set the curing time of each layer as 9 s and the curing thickness as 0.05 mm. The morphology of solid luminescent materials determines the number of cured layers.

AIE performance measurement

In this paper, the fluorescence spectra of the synthesized compounds in different ratio solutions were measured and recorded on an F-4500 (Hitachi High-Technologies Corporation) fluorescence spectrophotometer. 10 groups of 10 mL tetrahydrofuran aqueous solutions with a concentration of 5×10^{-5} M were prepared. The volume content of water in each group was 90%, 80%, 70%, 60%, 50%, 40%, 30%, 20%, 10%, and 0%, respectively. At the same time, different ratios of solutions were irradiated under a 365 nm LED to obtain fluorescence photos.

Synthesis of fluorescent dyes

The general synthetic procedures toward tetrastyrene-based derivatives Cz-bi-Ph, Cz-hex-Ph, DHBF-Ph, and BP-Ph, are outlined in Fig. 1. In general, tetrastyrene-based products are obtained through a two-step reaction, including Friedel–Crafts acylation and McMurry reaction.

Under ice bath conditions, the starting materials, namely *N*-ethylcarbazole (2.0 g, 10 mmol), *N*-hexylcarbazole (2.5 g, 10 mmol), dihydrobenzofuran (1.2 g, 10 mmol), and biphenyl (1.5 g, 10 mmol) were added to a 50 mL one-neck flask in the presence of aluminum trichloride (1.3 g, 10 mmol) using dichloromethane as a solvent. Benzoyl chloride (1.4 g, 10 mmol) was slowly added dropwise under magnetic stirring, and the reaction system was monitored by thin-layer chromatography. After the reaction was completed, the reaction solution was quenched with water, and the organic phase was extracted with
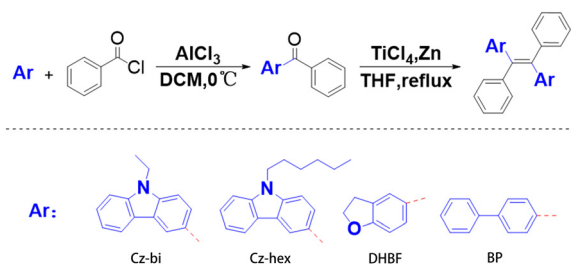
Fig. 1 Synthetic routes of tetrastyrene derivatives.

an appropriate amount of dichloromethane. The organic phase was washed three times with saturated brine, then dried with anhydrous MgSO$_4$, and finally, the solvent was evaporated by rotary evaporation to obtain a crude product. The crude product was purified by silica gel chromatography to give the pure product of the ketone derivatives.

Titanium tetrachloride (4.75 g, 25 mmol) was added to a solution of zinc powder (2.6 g, 40 mmol) in dry tetrahydrofuran (20 mL) at 0 °C under a nitrogen atmosphere. The solution was stirred at this temperature for 5 minutes, and then the ketone derivative, namely (9-ethylcarbazol-2-yl)-phenylmethanone (3.0 g, 10 mmol), (9-hexylcarbazol-2-yl)-phenylmethanone (3.5 g, 10 mmol), (2,3-dihydrobenzofuran-6-yl)(phenyl)methanone (2.3 g, 10 mmol), and [1,1′-biphenyl]-4-yl(phenyl)methanone (2.6 g, 10 mmol), was added to the solution. The system was heated to reflux, and the progress of the reaction was monitored by thin layer chromatography. After the reaction of the raw materials was complete, the reaction mixture was quenched with ice water, and the organic phase was extracted with methylene chloride. The organic layer was washed three times with saturated Na$_2$CO$_3$ solution and water. The organic phase was dried on anhydrous MgSO$_4$. The solvent was evaporated by rotation to obtain the crude product. The crude product was purified by column chromatography. The Cz-bi-Ph was obtained as a yellow-green solid with a quantity of 1.70 g. The Cz-hex-Ph was obtained as a yellow-green solid with a quantity of 1.56 g. The DHBF-Ph was obtained as a white solid with a quantity of 1.78 g. The BP-Ph was obtained as a yellow solid with a quantity of 1.63 g. NMR and IR characterization data of all dyes are shown in ESI.†

(**E**)-1,2-bis(9-ethyl-9**H**-carbazol-3-yl)-1,2-diphenylethene (Cz-bi-Ph). ¹H NMR (400 MHz, CDCl$_3$) δ 7.91 (dd, J = 15.6, 7.7 Hz, 2H), 7.86 (dd, J = 5.5, 1.6 Hz, 2H), 7.49–7.34 (m, 4H), 7.31–7.26 (m, 2H), 7.24–7.14 (m, 10H), 7.13 (s, 4H), 4.33 (q, J = 7.2 Hz, 2H), 4.26 (q, J = 7.2 Hz, 2H), 1.46 (t, J = 7.2 Hz, 3H), 1.39 (t, J = 7.2 Hz, 3H). ¹³C NMR (101 MHz, CDCl$_3$) δ 144.84, 140.78, 140.20, 138.66, 135.24, 131.78, 130.02, 129.86, 127.60, 126.08, 125.32, 123.57, 123.10, 122.51, 120.49, 118.69, 108.43, 107.55, 36.11, 13.91. IR (KBr, v(cm^{-1})): 3049 (–C=C–H); 2974 (CH3–); 2931 (–CH2–); 1597 (–CH=CH–); 1490, 1477 (Ar–H).

(**E**)-1,2-bis(9-hexyl-9**H**-carbazol-3-yl)-1,2-diphenylethene (Cz-hex-Ph). ¹H NMR (400 MHz, CDCl$_3$) δ 7.99–7.82 (m, 4H), 7.51–7.36 (m, 4H), 7.32 (d, J = 6.9 Hz, 2H), 7.28–7.08 (m, 14H), 4.27 (dd, J = 20.5, 13.3 Hz, 4H), 1.96–1.80 (m, 4H), 1.46–1.30 (m, 12H), 0.95 (dt, J = 17.7, 6.9 Hz, 6H). ¹³C NMR (101 MHz, CDCl$_3$) δ 145.74, 140.70, 140.36, 139.23, 135.16, 131.85, 130.70, 127.63, 126.06, 125.32, 123.49, 123.05, 122.44, 119.89, 118.61, 108.68, 106.43, 43.17, 34.65, 29.53, 26.21, 22.61, 11.74. IR (KBr, v(cm^{-1})): 3054 (–C=C–H); 2953, 2927 (CH$_3$–CH$_2$–); 2853 (–CH$_2$–); 1597 (–CH=CH–); 1484, 1443 (Ar–H).

(**E**)-1,2-bis(2,3-dihydrobenzofuran-5-yl)-1,2-diphenylethene (DHBF-Ph). ¹H NMR (400 MHz, CDCl$_3$) δ 7.15–7.05 (m, 8H), 7.05–7.01 (m, 2H), 6.87–6.73 (m, 4H), 6.52 (dd, J = 18.0, 8.2 Hz, 2H), 4.50 (q, J = 8.7 Hz, 4H), 3.03 (dt, J = 16.6, 8.6 Hz, 4H). ¹³C NMR (101 MHz, CDCl$_3$) δ 155.70, 145.32, 139.87, 137.07, 132.44, 130.99, 127.91, 127.82, 127.65, 127.56, 126.23, 126.20, 126.09, 108.45, 70.25, 29.57. IR (KBr, v(cm^{-1})): 3049 (–C=C–H); 2974 (CH$_3$–); 2931 (–CH$_2$–); 1597 (–CH=CH–); 1490, 1477 (Ar–H).

(**E**)-1,2-di([1,1′-biphenyl]-4-yl)-1,2-diphenylethene (BP-Ph). ¹H NMR (400 MHz, CDCl$_3$) δ 7.59 (d, J = 9.7 Hz, 4H), 7.42 (q, J = 8.0 Hz, 8H), 7.37–7.29 (m, 3H), 7.28–7.24 (m, 1H), 7.20–7.10 (m, 12H). ¹³C NMR (101 MHz, CDCl$_3$) δ 144.39, 142.79, 141.12, 138.99, 131.83, 131.48, 128.71, 128.42, 128.27, 127.83, 127.72, 127.19, 126.89, 126.52, 126.33, 126.22. IR (KBr, v(cm^{-1})): 3026 (–C=C–H); 1597 (–CH=CH–); 1487, 1441 (Ar–H).

Results and discussion

Photocuring with TPO as a photoinitiator

Solid luminescent materials by DLP printing and fluorescence properties of dyes. To obtain solid luminescent materials by DLP printing, Cz-bi-Ph, Cz-hex-Ph, DHBF-Ph, and BP-Ph were used as fluorescent dyes in the 3D printing formula. The
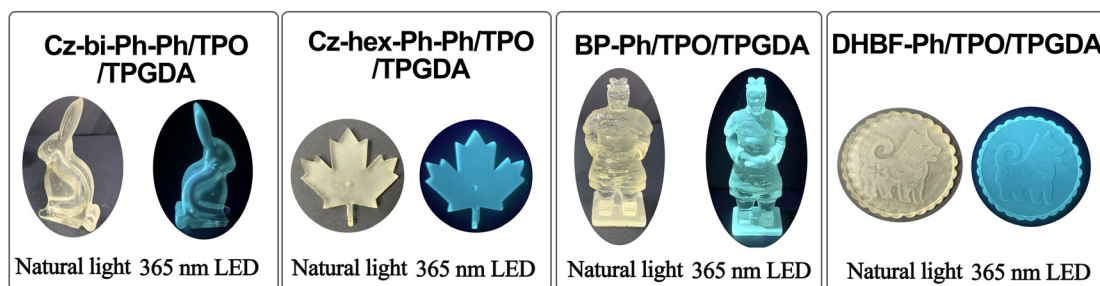

Fig. 2 The pictures of the 3D printed model under natural light and 365 nm LED (TPO: 0.5 wt%, dyes: 0.5 wt%, NMP (N-methyl pyrrolidone, solvent): 1.0 wt%, TPGDA: 98.0 wt%. The dimensions of the printed objects from left to right are 4 cm × 2 cm × 6 cm, 5 cm × 5 cm × 2 cm, 4 cm × 2 cm × 6 cm, 5 cm × 5 cm × 2 cm in length, width and height).

obtained models were successfully printed with a high resolution and a strong blue fluorescence (Fig. 2), indicating that fluorescence from these dyes was not quenched in the solid state after the photocuring process. To investigate the fluorescence properties of the dyes in a solution, the fluorescence intensity changes of the dyes in a THF/water solution were tested. Four dyes showed a weak fluorescence intensity in the THF solution but exhibited extreme fluorescence intensity after the addition of different water fractions. Fig. 3(a) indicates that the fluorescence intensity starts to rise when the water fraction is greater than 60%, and the change in fluorescence intensity can be seen in the photos (Fig. 3(b)). The solubility of the dyes in the solution decreases with increasing water fraction, leading to the aggregation of the molecules, which causes the fluorescence intensity to increase.[33] These tetrastyrene-based dyes show classic AIE characteristics. The fluorescence of the model is determined by the AIE properties of the dyes in the formulation.

Effect of the dyes on the photoinitiation activity of TPO. To investigate the effect of the dyes on the photoinitiation activity of TPO in FRP, TPGDA photocuring was carried out under a 405 nm LED. The conversion rates of TPGDA under different irradiation times were obtained, as shown in Fig. 4(a). We found that both Cz-bi-Ph and Cz-hex-Ph have absorption at 405 nm, so they compete with TPO for light energy, causing lower conversions for the Cz-bi-Ph/TPO and Cz-hex-Ph/TPO systems compared to the TPO system. In contrast, the DHBF-Ph/TPO and BP-Ph/TPO systems showed little change, implying that the addition of dyes slightly affected the initiation activity of TPO to varying degrees. The UV-vis absorption spectra of TPO and the dyes are shown in Fig. 4(b). Both TPO and the dyes absorb at 405 nm, and this leads to competition between them for light energy and causes some decrease in the photocuring rate of the TPGDA initiated by TPO. As we can see in Fig. 4(b), Cz-bi-Ph has a higher absorption intensity at 405 nm than Cz-hex-Ph, resulting in less light energy obtained by TPO in the Cz-bi-Ph systems and a slower polymerization rate. The higher the dyes' absorption intensity is at 405 nm, the lower the corresponding photocuring conversion is.

Photostability of the dyes during the photocuring process. For fluorescent dyes, stability is vital during the photocuring process. To further study the photostability of the dyes during
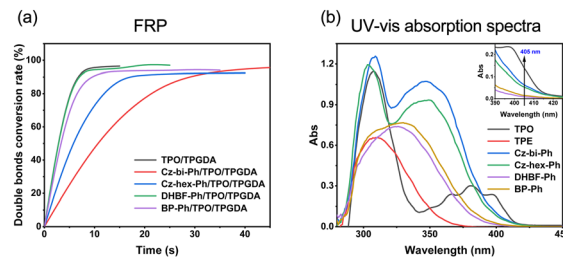

Fig. 4 (a) Photocuring profiles of TPGDA in the presence of TPO and dyes/TPO under a 405 nm LED (TPO: 0.5 wt%, dyes: 0.5 wt%, NMP: 1.0 wt%, TPGDA: 98.0 wt%). (b) UV-Vis spectra of TPO and the dyes in THF solution ($c = 5 \times 10^{-4}$ M).

the photocuring process, we tested the steady-state photolysis of TPO, the dyes, and dyes/TPO at different irradiation times under a 405 nm LED, as shown in Fig. 5. We found that the absorption peaks of TPO decreased rapidly at 310 and 380 nm with the irradiation time. In the photolysis of dyes/TPO, the absorption peak decreased at 380 nm but did not change greatly at 310 nm after the dyes/TPO were irradiated for 50 s. Fig. S1 (ESI†) shows the steady-state photolysis of the dyes. After irradiation for 300 s, the absorption peaks of the dyes did not change, indicating that the dyes would not cause photolysis. The results show that the dyes have a good photostability during the photocuring of the TPDGA initiated by TPO.

Change of fluorescence intensity with the irradiation period. To determine whether dyes can be used as fluorescent probes to monitor photocuring, we investigated the fluorescence spectra of the dyes/TPO/TPGDA system at different irradiation times. Fig. 6 shows that the fluorescence spectrum of the dyes/TPO/TPGDA system changes with the irradiation time. Within 0 to 5 s, the fluorescence intensity increased with the irradiation period. At about 10 s, the fluorescence intensity of photocuring tended to stabilize after a while, indicating the end of the photocuring process. In the photocuring process, the viscosity of the system changes with increasing irradiation time, the free rotation of the dyes in the system is limited, and the fluorescence intensity increases accordingly. In addition, due to the AIE characteristics of the dyes, the fluorescence intensity changes of the dyes/TPO system vary. The fluorescence intensity of the DHBF-Ph/TPO and BP-Ph/TPO systems displays the most significant change. The above discussions support the use of dyes with AIE characteristics as a fluorescent probe to monitor photocuring and as fluorescent dyes to fabricate solid luminescent materials in 3D printing.

Photocuring with the dye-sensitized photoinitiation system

Photosensitizing activity of the dyes to ONI in FRP. The dye-sensitized photoinitiation system is vital in LED-driven photopolymerization. To investigate the photosensitizing properties of Cz-bi-Ph, Cz-hex-Ph, DHBF-Ph, and BP-Ph, the photopolymerization of three kinds of free radical monomers, namely TMPTA, TPGDA, and PEGDA with ONI as a photoinitiator, was investigated under a 405 nm LED light source. Due to it exhibiting no absorption at 405 nm, ONI cannot initiate the
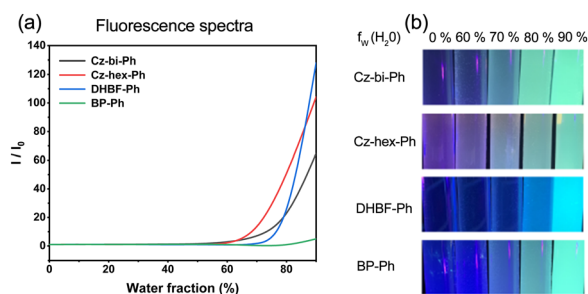

Fig. 3 (a) Changes of fluorescence intensity of the dyes in the THF/water (0–90 vol%) solution; (b) photo of the dyes in different water fraction mixtures under 365 nm LED ($c = 5 \times 10^{-5}$ M).
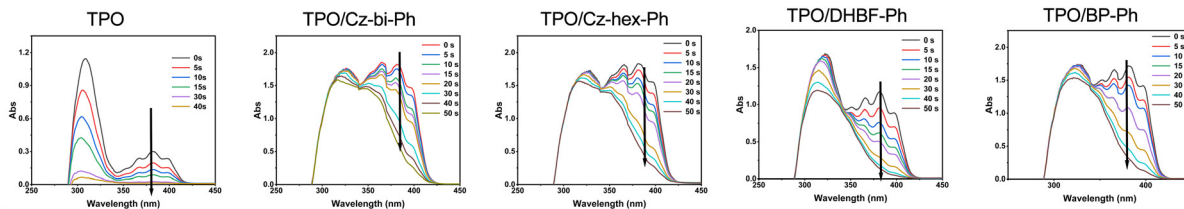
Fig. 5 Steady-state photolysis of TPO and dyes/TPO with different irradiation times in THF solution (TPO: 5×10^{-5} M, dyes: 5×10^{-5} M).
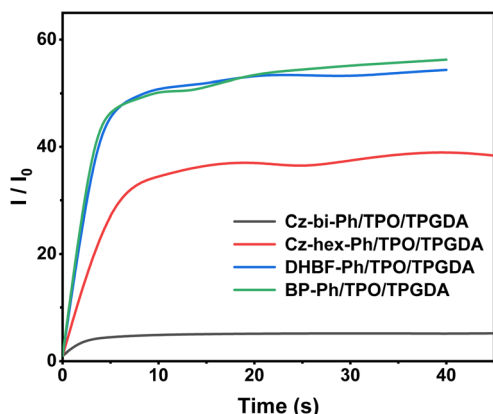

Fig. 6 Changes of fluorescence intensity of the dyes/TPO/TPGDA in FRP at different irradiation times.

photocuring under a 405 nm LED. Fig. 7 shows the double bond conversion of monomers with the irradiation time. For comparison, the photoactivity of tetraphenylethene (TPE) was also tested under the same conditions.

We found that the photocuring did not proceed using TPE as the photosensitizer of ONI, which is related to the non-absorption of TPE at 405 nm. However, photocuring can occur using Cz-bi-Ph, Cz-hex-Ph, DHBF-Ph, and BP-Ph as photosensitizers. The conversion rates of the photocuring systems increased with the irradiation time. The Cz-bi-Ph/ONI and Cz-hex-Ph/ONI systems had the fastest conversion rates. The conversion of TPGDA exceeded 90%, that of PEGDA finally reached 92%, and that of TMPTA reached 78% at 90 s. Photocuring is affected by the functionality and viscosity of the resin. High-functionality TMPTA can accelerate the polymerization reaction. Nevertheless, TMPTA with high density will rapidly form a 3D network structure, leading to the encapsulation of active radicals and unreacted TMPTA monomers in the cross-linked network.[42] Given the limitations, the double bond conversion at the equilibrium of dyes/ONI/TMPTA is significantly lower than that of TPGDA and PEGDA.

Taking the dyes/ONI/TPGDA as an example, Fig. 7(b) shows that the sensitizing activity of the dye to ONI is Cz-hex-Ph ≈ Cz-bi-Ph > DHBF-Ph > BP-Ph. The UV-vis absorption intensity and molecular structure of the dyes determine the sensitizing activity of the dyes/ONI. Cz-bi-Ph and Cz-hex-Ph absorb light energy with high efficiency because the UV-vis absorption intensity of Cz-bi-Ph and Cz-hex-Ph at 405 nm is greater than that of BP-Ph and DHBF-Ph. Although the absorption intensity

of DHBF-Ph is not as strong as that of BP-Ph, DHBF-Ph has electron-donating groups. Consequently, the sensitizing activity of DHBF-Ph is higher than that of BP-Ph.

Photosensitizing activity of the dyes to ONI in CP. The cationic polymerization of epoxy oligomer E51 initiated by dyes/ONI was investigated under a 405 nm LED. Fig. 7(d) shows the conversion of cationic polymerization (CP) *versus* irradiation time. Under a 405 nm LED, TPE/ONI can hardly induce CP, indicating that TPE has no sensitizing effect on ONI in CP. The Cz-hex-Ph/ONI system has the highest initiating activity, and the conversion rate of E51 can reach 90% after irradiation for 150 s. Meanwhile, those of Cz-bi-Ph/ONI, DHBF-Ph/ONI, and BP-Ph/ONI reached 70%. The results show that Cz-hex-Ph/ONI has better priming activity in CP than other dyes/ONI systems. Cz-bi-Ph/ONI and Cz-hex-Ph/ONI have a lower priming activity in CP than FRP, which may be due to the alkalinity of the carbazolyl groups contained in Cz-bi-Ph and Cz-hex-Ph.

Photosensitizing and photoinitiation mechanism. Electrochemical properties are essential for evaluating the feasibility of photoinduced electron transfer reactions and the redox reversibility of the photocatalysts. Therefore, cyclic voltammetry experiments were performed on Cz-bi-Ph, Cz-hex-Ph, DHBF-Ph, and BP-Ph. The results are shown in Fig. 8(a), and the corresponding electrochemical data are shown in Table 1. The experimental results show that Cz-bi-Ph has the lowest oxidation potential and is easily oxidized by ONI. This phenomenon is also one of the reasons for the excellent photoinitiated activity of Cz-bi-Ph/ONI during photocuring. The free energy change (ΔG_T) for electron transfer between the excited dye and ONI is calculated using the classical Rehm–Weller equation as follows:

$$\Delta G_T = E_{ox} - E_{red} - E_s - C$$

In this equation, E_{ox}, E_{red}, E_s, and C are the oxidation potential of the dyes, the reduction potential of ONI, the excited singlet state energy of the dyes, and the electrostatic interaction energy for the initially formed ion pair, respectively. The calculated ΔG_T values are all negative (Table 1), indicating the thermodynamically favored photoinduced electron transfer.

According to the above experimental results, a reasonable reaction mechanism is proposed. As shown in Fig. 8(c), dyes were first excited under light irradiation. The excited dyes and the ground state ONI generated radical cations and $(CH_3)_2Ph^\bullet$ through electron transfer. $(CH_3)_2Ph^\bullet$ decomposed to generate $CH_3Ph^\bullet$, which then initiated FRP. In the presence
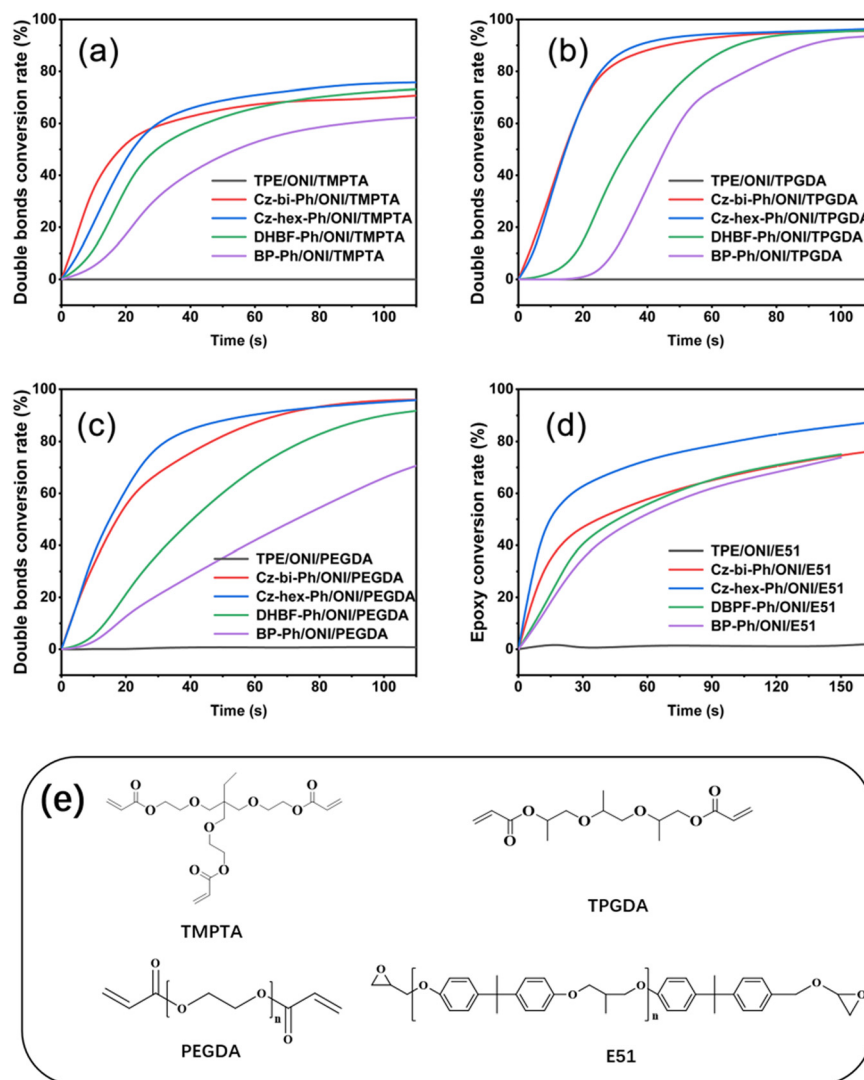
Fig. 7 Photocuring profiles of (a) TMPTA, (b) TPGDA and (c) PEGDA in the presence of dyes/ONI under a 405 nm LED (dyes: 0.5 wt%, ONI: 3 wt%, NMP: 3.0 wt%, resin: 93.5 wt%). (d) Photocuring profiles of E51 in the presence of dyes/ONI under a 405 nm LED (dyes: 0.5 wt%, ONI: 3 wt%, ECH (epichlorohydrin, solvent): 3.0 wt%, E51: 93.5 wt%). (e) The chemical structures of TMPTA, TPGDA, PEGDA and E51.

of hydrogen-donating (R-H) compounds, radical cations extracted hydrogen protons to form Brønsted acids, which initiated CP.

Fluorescence emission during the FRP and CP process. The fluorescence spectra during FRP and CP process initiated by the dyes/ONI were tested. As shown in Fig. S2 (ESI†), the fluorescence intensity at its emission maxima increased with the illumination. Fig. 8(b) shows the fluorescence intensity changes of the dyes/ONI/TPGDA system. The fluorescence changes of the Cz-bi-Ph/ONI and Cz-hex-Ph/ONI systems tended to be stable at 25 s, and the DHBF-Ph/ONI and BP-Ph/ONI systems tended to be stable at 80 and 90 s, respectively. This phenomenon is consistent with the changes in the photocuring rates with the irradiation time. Finally, the fluorescence intensity of all the systems decreased slowly, which may be caused by the consumption of the dye molecules during the photocuring process, which weakened the AIE effect. The results show that

all dyes can also be used as fluorescent probes to monitor the photocuring while sensitizing ONI.

As shown in Fig. 9, the dyes/ONI/TPGDA system has no fluorescence at 0 s and a fluorescence enhancement at 40 s. The Cz-bi-Ph/ONI/TPGDA system has a weak fluorescence, and the fluorescence intensity of the system does not change significantly with increasing irradiation time. Given the high viscosity of the E51 system, the free rotation of dyes in the system is limited, resulting in obvious fluorescence, which is shown in Fig. S3 (ESI†).

Conclusion

We synthesized four tetraarylethene dyes with the carbazole, dihydrobenzofuran, or biphenyl group. These dyes exhibit photosensitization activity and can be used as fluorescent dyes
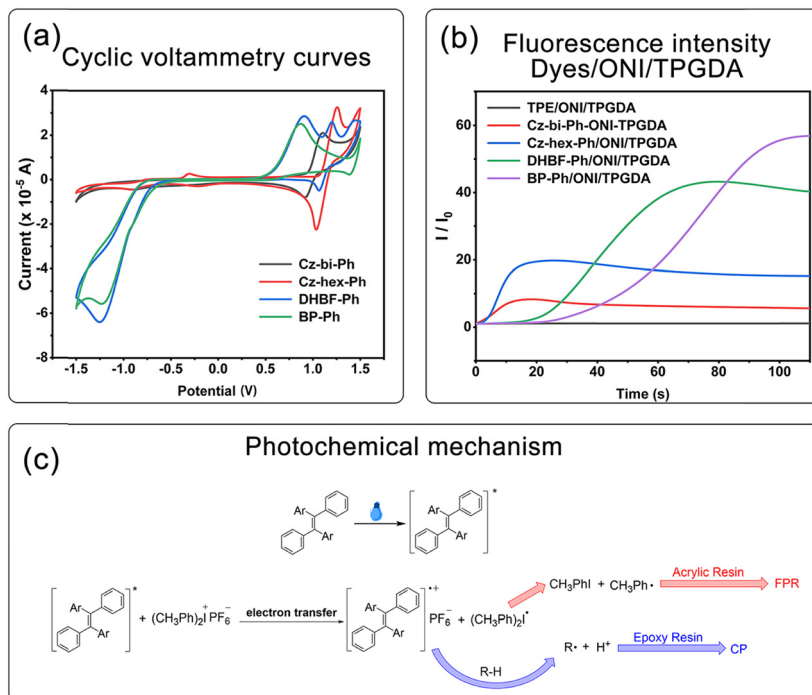
Fig. 8 (a) Cyclic voltammetry curves of the dyes ($c = 1 \times 10^{-3}$ M). (b) Changes of fluorescence intensity of the dyes/ONI/TPGDA in photocuring at different irradiation times. (c) Photochemical mechanisms of the generation of initiating radicals/cations in dyes/ONI involved in the current paper.

Table 1 Parameters characterizing the photochemical reactivity of the proposed dyes/ONI

	E_{ox}	E_{ONI}	E_s	ΔG_T
Cz-bi-Ph	0.48	0.19	3.35	−3.06
Cz-hex-Ph	0.44	0.19	3.40	−3.14
BP-Ph	1.43	0.19	3.32	−2.08
DHBF-Ph	0.50	0.19	3.33	−3.02

E_{OX} values *vs.* SCE (E (Fc$^+$/Fc) = 0.38 V[43] *vs.* SCE, E (Fc$^+$/Fc) = 0.13 V *vs.* Ag$^+$/Ag), E_{ONI} = −0.19 V.[44]

in LED photocuring. Using these dyes as fluorescence dyes in the 3D printing formula, the models with high resolution and strong blue fluorescence were successfully printed from DLP printers. These dyes show AIE properties and can thus be used as a fluorescent probe to monitor the photocuring process. The sensitizing activities of Cz-hex-Ph and Cz-bi-Ph are more potent than those of DHBF-Ph and BP-Ph. The fluorescence strength of DHBF-Ph and BP-Ph is higher than that of Cz-hex-Ph and Cz-bi-Ph, making DHBF-Ph and BP-Ph more suitable as fluorescent probes for obtaining solid luminescent materials through DLP printing. TPEs as AIE molecules can be introduced into resin monomers to monitor polymerization or for the preparation of solid luminescent materials in 3D printing materials. The absorption of TPE molecules is low, so it is possible to prolong the absorption range by introducing different electron-assigned groups of carbazole, phenothiazine, *etc.* or by increasing the degree of conjugate, and then sensitizing the chain salts as photosensitizers to induce polymerization.
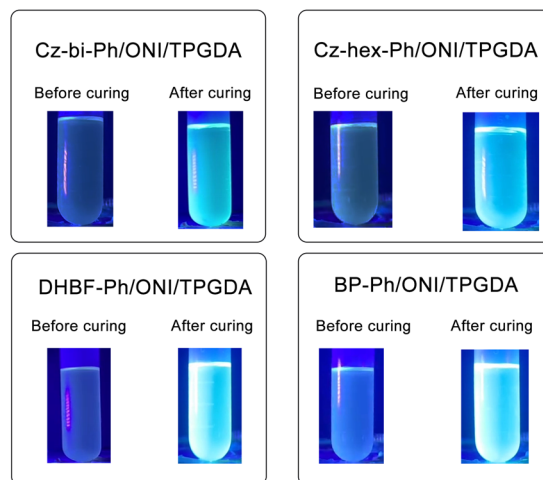

Fig. 9 Fluorescence images of the dyes/ONI/TPGDA system before and after illumination for 40 s (dyes: 0.5 wt%, ONI: 3 wt%, NMP: 3.0 wt%, TPGDA: 93.5 wt%).

Author contributions

Dongxiao Li: conceptualization, methodology, formal analysis, investigation, writing – original draft, writing – review & editing. Yimei Liu: investigation. Binghui Bao: investigation. Yao Du: investigation. Jian You: investigation. Luhang Zhang: investigation. Haitao Zhan: investigation. Tao Wang: conceptualization, resources, writing – review & editing, supervision, funding acquisition.

Conflicts of interest

The authors declare no competing financial interest.

Acknowledgements

Notes and references

1 M. Gastaldi, F. Cardano, M. Zanetti, G. Viscardi, C. Barolo, S. Bordiga, S. Magdassi, A. Fin and I. Roppolo, *ACS Mater. Lett.*, 2021, **3**, 1–17.

2 F. Ciardelli, G. Ruggeri and A. Pucci, *Chem. Soc. Rev.*, 2013, **42**, 857–870.

3 M. Carlotti and V. Mattoli, *Small*, 2019, **15**, 1902687.

4 A. Reisch and A. S. Klymchenko, *Small*, 2016, **12**, 1968–1992.

5 R. Pei, L. Fan, F. Zhao, J. Xiao, Y. Yang, A. Lai, S.-F. Zhou and G. Zhan, *J. Hazard. Mater.*, 2020, **384**, 121418.

6 J. Shojaeiarani, A. Shirzadifar and D. S. Bajwa, *Microporous Mesoporous Mater.*, 2021, **327**, 111382.

7 D. Dean, E. Mott, X. Luo, M. Busso, M. O. Wang, C. Vorwald, A. Siblani and J. P. Fisher, *Virtual Phys. Prototyping*, 2014, **9**, 3–9.

8 I. Xenikakis, M. Tzimtzimis, K. Tsongas, D. Andreadis, E. Demiri, D. Tzetzis and D. G. Fatouros, *Eur. J. Pharm. Sci.*, 2019, **137**, 104976.

9 P. Theato, B. S. Sumerlin, R. K. O'Reillyc and T. H. Epps, *Chem. Soc. Rev.*, 2013, **42**, 7055.

10 T. Ube and T. Ikeda, *Adv. Opt. Mater.*, 2019, **7**, 1900380.

11 S. Nocentini, D. Martella, C. Parmeggiani and D. S. Wiersma, *Adv. Opt. Mater.*, 2019, **7**, 1900156.

12 Y. Zhang, Y. Xu, A. Simon-Masseron and J. Lalevée, *Chem. Soc. Rev.*, 2021, **50**, 3824–3841.

13 T. D. Ngo, A. Kashani, G. Imbalzano, K. T. Q. Nguyen and D. Hui, *Composites, Part B*, 2018, **143**, 172–196.

14 P. Garra, J. P. Fouassier, S. Lakhdar, Y. Yagci and J. Lalevée, *Prog. Polym. Sci.*, 2020, **107**, 101277.

15 V. Y. Chang, C. Fedele, A. Priimagi, A. Shishido and C. J. Barrett, *Adv. Opt. Mater.*, 2019, **7**, 1900091.

16 W. Xu, S. Jambhulkar, Y. Zhu, D. Ravichandran, M. Kakarla, B. Vernon, D. G. Lott, J. L. Cornella, O. Shefi, G. Miquelard-Garnier, Y. Yang and K. Song, *Composites, Part B*, 2021, **223**, 109102.

17 S. Patra and V. Young, *Cell Biochem. Biophys.*, 2016, **74**, 93–98.

18 N. J. Findlay, J. Bruckbauer, A. R. Inigo, B. Breig, S. Arumugam, D. J. Wallis, R. W. Martin and P. J. Skabara, *Adv. Mater.*, 2014, **26**, 7290–7294.

19 Z. Shi, C. Xu, F. Chen, Y. Wang, L. Li, Q. Meng and R. Zhang, *RSC Adv.*, 2017, **7**, 49947–49952.

20 R. Mazzaro and A. Vomiero, *Adv. Energy Mater.*, 2018, **8**, 1801903.

21 T. Mikulchyk, S. Martin and I. Naydenova, *Opt. Mater.*, 2014, **37**, 810–815.

22 G. Yilmaz, G. Acik and Y. Yagci, *Macromolecules*, 2012, **45**, 2219–2224.

23 H. Chen, G. Noirbent, K. Sun, D. Brunel, D. Gigmes, F. Morlet-Savary, Y. Zhang, S. Liu, P. Xiao, F. Dumur and J. Lalevée, *Polym. Chem.*, 2020, **11**, 4647–4659.

24 W. Tomal, A. Chachaj-Brekiesz, R. Popielarz and J. Ortyl, *RSC Adv.*, 2020, **10**, 32162–32182.

25 F. Wang, Y. Chong, F. Wang and C. He, *J. Appl. Polym. Sci.*, 2017, **134**, 44988.

26 J. Qi, X. Hu, X. Dong, Y. Lu, H. Lu, W. Zhao and W. Wu, *Adv. Drug Delivery Rev.*, 2019, **143**, 206–225.

27 S. K. Samanta, K. Maiti, S. K. Manna, S. S. Ali, U. N. Guria, A. Ghosh, P. Datta and A. K. Mahapatra, *Dyes Pigm.*, 2021, **196**, 109758.

28 H. Wang, H. Xing, J. Gong, H. Zhang, J. Zhang, P. Wei, G. Yang, J. W. Y. Lam, R. Lu and B. Z. Tang, *Mater. Horiz.*, 2020, **7**, 1566–1572.

29 L. Zong, Y. Xie, C. Wang, J.-R. Li, Q. Li and Z. Li, *Chem. Commun.*, 2016, **52**, 11496–11499.

30 H. Lu, K. Wang, B. Liu, M. Wang, M. Huang, Y. Zhang and J. Yang, *Mater. Chem. Front.*, 2019, **3**, 331–338.

31 J. Yang, Z. Chi, W. Zhu, B. Z. Tang and Z. Li, *Sci. China: Chem.*, 2019, **62**, 1090–1098.

32 Z. Zhao, H. Zhang, J. W. Y. Lam and B. Z. Tang, *Angew. Chem., Int. Ed.*, 2020, **59**, 9888–9907.

33 X. Fan, Q. Xia, Y. Zhang, Y. Li, Z. Feng, J. Zhou, J. Qi, B. Z. Tang, J. Qian and H. Lin, *Adv. Healthcare Mater.*, 2021, **10**, 2101043.

34 T. Han, D. Yan, Q. Wu, N. Song, H. Zhang and D. Wang, *Chin. J. Chem.*, 2021, **39**, 677–689.

35 Y. Hong, *Methods Appl. Fluoresc.*, 2016, **4**, 022003.

36 Z. Liu, J. Liu, X. Wang, F. Mi, D. Wang and C. Wu, *Bioconjugate Chem.*, 2020, **31**, 1857–1872.

37 M. A. Auwalu and S. Cheng, *Chemosensors*, 2021, **9**, 44.

38 G. R. Suman, M. Pandey and A. S. J. Chakravarthy, *Mater. Chem. Front.*, 2021, **5**, 1541–1584.

39 J. Yang, M. Fang and Z. Li, *Aggregate*, 2020, **1**, 6–18.

40 F. Zhao, Z. Chen, C. Fan, G. Liu and S. Pu, *Dyes Pigm.*, 2019, **164**, 390–397.

41 D. Zhao, J. You, H. Fu, T. Xue, T. Hao, X. Wang and T. Wang, *Polym. Chem.*, 2020, **11**, 1589–1596.

42 H. Zou, S. Wu and J. Shen, *Chem. Rev.*, 2008, **108**, 3893–3957.

43 V. V. Pavlishchuk and A. W. Addison, *Inorg. Chim. Acta*, 2000, **298**, 97–102.

44 H. E. Bachofner, F. M. Beringer and L. Meites, *J. Am. Chem. Soc.*, 1958, **80**, 4269–4274.